1998

Launch Detection Satellite System Engineering Error Analysis

Beaulieu, M.R.; Alfriend, K.T.; Jerardi, T.

AIAA

Beaulieu, Martin Ronald, K. T. Alfriend, and Thomas Jerardi. "Launch detection satellite system engineering error analysis." Journal of spacecraft and rockets 35.4 (1998): 487-495.
http://hdl.handle.net/10945/69586

JOURNAL OF SPACECRAFT AND ROCKETS
Vol. 35, No. 4, July–August 1998

Launch Detection Satellite System Engineering Error Analysis

M. R. Beaulieu* and K. T. Alfriend†
U.S. Naval Postgraduate School, Monterey, California 93943
and
T. Jerardi‡
Johns Hopkins University, Applied Physics Laboratory, Laurel, Maryland 20723-6099

An orbiting detector of infrared energy may be used to detect the rocket plumes generated by ballistic missiles during the powered segment of their trajectory. By measuring the angular directions of arrival of the detections over several observations, the trajectory properties, launch location, and impact area may be estimated using a nonlinear least-squares iteration procedure. Observations from two or more sensors may be combined to form stereoscopic lines of sight, increasing the accuracy of the algorithm. A computer model is presented of an estimation algorithm that determines what parameter, or combination of parameters, will have a significant effect on the error of the tactical parameter estimation. This model generates observation data and then, using the data, produces an estimate of the tactical parameters, i.e., the time, position, and heading at launch and burnout, and an impact time and position. For the expected range of values of each of the error sources, the line-of-sight errors, a combination of focal-plane and attitude errors, had the greatest effect on the estimation of the launch and impact points.

Nomenclature

$\boldsymbol{A}$	= matrix of partials
$\boldsymbol{A}_1$	= matrix of partial derivatives of the spherical coordinates with respect to the tactical parameters
$\boldsymbol{A}_2$	= transformation from Earth-centered Cartesian frame to spherical coordinates
$\boldsymbol{A}_3$	= transformation from focal-plane Cartesian coordinates to Earth-centered Cartesian frame
$\boldsymbol{A}_4$	= transformation from focal-plane coordinates to focal-plane Cartesian coordinates
a_i, b_i	= coefficients in polynomial representation of tactical ballistic missile (TBM) downrange and altitude
alt	= altitude of TBM
d	= downrange distance of TBM
$\text{gha}_k, \delta_k, R_k$	= Greenwich hour angle, declination, and radius of the satellite
h	= height above WGS-84 ellipsoid
I_k, β_k, η_k	= radiant intensity, azimuth, and elevation of kth infrared return; β is measured clockwise from due South
L	= loft
R_e	= Earth radius
S/C_i	= ith Defense Support Program satellite
T	= time
T_{bo}	= TBM burnout time
T_k	= time of kth observation measured from midnight of the day of the observation, s
T_{last}	= time of last observation
T_{next}	= next potential observation time
t	= time of flight from TBM launch
$t_{\max}$	= TBM profile maximum burnout time
V	= TBM velocity
$\boldsymbol{W}$	= weight matrix
$\boldsymbol{x}$	= $(T_0, L, \phi_0, \lambda_0, h_0, \alpha_0)^T$, vector representing the tactical parameters
$\boldsymbol{x}_C$	= assumed initial values of the tactical parameters
y	= actual observations
y_O, y_C	= actual and calculated observations
α	= flight trajectory azimuth (true heading)
γ	= TBM flight-path angle
θ	= Earth central angle measured from launch
λ	= geodetic longitude
ϕ	= geodetic latitude
$()_{\text{bo}}$	= value of $()_{\text{bo}}$ at burnout
$()_0$	= value of $()_0$ at launch

Received Feb. 24, 1997; revision received Dec. 23, 1997; accepted for publication Feb. 9, 1998. This paper is declared a work of the U.S. Government and is not subject to copyright protection in the United States.

*Graduate Student, Space Systems Academic Group; currently Assistant Strike Operations Officer, USS *Carl Vinson*, U.S. Navy, Bremerton, WA.

†Navy TENCAP Chair; currently Professor and Head, Aerospace Engineering Department, Texas A&M University, College Station, TX 77843-3141. Fellow AIAA.

‡Professional Staff. Member AIAA.

Introduction

THE TRW-built Defense Support Program (DSP) satellites have been the spaceborne segment of NORAD's Tactical Warning and Attack Assessment system since the early 1970s. Using infrared (IR) detectors that sense the heat from missile plumes against the Earth background, these orbiting sentries detect ballistic missile launches. The DSP system provides near real-time detection information in support of the U.S. Department of Defense tactical warning and attack assessment mission and is supported by a network of fixed and mobile ground stations that process and disseminate information to military commanders worldwide. The Cold War mission of the DSP system was to detect massive intercontinental ballistic missile (ICBM) attacks. The U.S. response to such an attack only required timely and unambiguous warning, and missile flight times were much longer than the time required to launch a retaliatory attack. Precise radar tracks could be established with enough time to mitigate effects as much as technology allowed.

The current combat environment demands much more from launch detection satellites. The present threat is from tactical ballistic missiles (TBMs), which exhibit much cooler and shorter thrust times and possibly more depressed trajectories than those exhibited by ICBMs. TBMs can be launched from almost anywhere within a large geographical area of interest, with lofted or depressed trajectories. To attack the launcher and/or employ antiballistic missile (ABM) weapons or alert potential victims within the impact zone, the tactical parameters must be estimated faster and more accurately than was required for the massive ICBM launch. For budgetary reasons, the United States is forced to use the existing DSP system to counter the TBM threat into the beginning of the next century,[1] until the Space-Based Infrared System is operational. More rapid extraction of more precise information from these existing, technology-limited satellites must be accomplished in the interim. ABM systems, such as Patriot or Aegis, may be employed as ABM umbrellas in a tactical area of interest, provided they receive precise and timely cueing from DSP.

This raises the question: "How accurate is the information provided by DSP?" To answer this question, an engineering error analysis was performed to determine the following.

Which errors are present in the detection system?

Which errors have the greatest effect on the accuracy of DSP output information?

What are the effects of the errors, both individually and collectively, on the estimated launch and impact points?

These questions are addressed in this paper. The algorithm used by the tactical warning system (TALON SHIELD/ALERT) to determine the missile trajectory and predict the launch and impact points is modeled, the various errors are introduced, and their effect is determined both analytically (statistically) and numerically by simulation. The presented results are taken from Ref. 2.

This paper differs from the earlier work by Danis,[3] who considered the estimation of the launch point and trajectory from just two observations. In addition, in this paper the errors in impact time and point are analyzed and the approach is different.

DSP

The DSP[4] system consists of one or more satellites in geosynchronous orbit and one or more ground receiving stations. The DSP satellite is 10 m long and 7 m in diameter and weighs over 2300 kg (Fig. 1). Each satellite is spun at 6 rpm along its longitudinal axis with the telescope pointing toward Earth so that the sensor scans Earth. A counter-rotating wheel keeps the system in a nominal zero-momentum state. This configuration is sometimes called a yaw spinner. The IR telescope is tilted from the spin axis, so that the photoelectric cell (PEC) array covers the radius of the Earth. As the satellite rotates, the entire surface of the Earth within the field of view (FOV) is scanned by the IR detector, as shown in Figs. 2 and 3.

Detection of IR sources is accomplished with the telescope and PEC array portions of the sensor. The PEC array of the IR detector is mounted with the nadir end at the center of the rotation of the telescope (Fig. 2). The array contains over 6000 detector cells that are sensitive to energy in the IR wavelengths. As the PEC array scans the FOV, a cell passing across an IR source will generate a voltage with an amplitude proportional to the signal intensity. This voltage signal is termed an IR return and is transmitted to ground processing stations after amplification and background filtering. Line of sight (LOS) of the IR source relative to the satellite is determined from the angle of rotation of the telescope at the time of detection, and the cell is illuminated.

Error Analysis Algorithm

The quality of the trajectory estimation process is of paramount importance to tactical ballistic missile defense (TBMD). Real-time knowledge of the launch position allows targeting of the launcher. Cueing for ABM systems, such as Patriot and Aegis, requires timely and accurate trajectory information, which can be propagated from knowledge of the state vector at burnout. Impact time and position are extrapolated from the state vector at burnout and can be used for warning personnel within the target area. Understanding the algorithms and equations employed in the estimation process is necessary to assess the quality of the estimated parameters.

The detection of a TBM launch is the starting point for any ballistic missile defense. DSP does this by detecting IR radiation emitted by the exhaust plume of a launching missile. With detections by two or more spacecraft (stereo), triangulation of LOS can be used to more accurately estimate the boost-phase trajectory, which then is used to calculate launch position, state vector (position and velocity) at engine burnout, and impact position.

The tactical parameter estimation process is composed of several tasks: initial estimate of the tactical parameters, nonlinear least-squares estimation (refinement) of the tactical parameters, burnout time estimation, state vector generation, and impact point calculation. The tactical parameters are discussed in the following subsections.

Observational Data

From the observational data, the LOS relative to the satellite is determined. With the attitude data that are included in the telemetry and the satellite position as determined by the Air Force Satellite Control Network (AFSCN), the LOS from the satellite to the IR event in Earth-centered coordinates can be determined. Table 1 shows the first few of a typical set of observations of a single TBM launch.

The index k runs from 1 to n, the total number of observations, and is used as a subscript for the remaining symbols to denote a particular observation. The Spacecraft Identification, S/C ID, identifies which satellite is making the observation. In this example the event was detected by three satellites. The type of TBM being detected is determined from the intensity I_k. The other parameters are shown in Figs. 4 and 5.

TBM Profile

A TBM profile is a description of the nominal powered flight trajectory of a given TBM. A profile consists of IR intensity and the

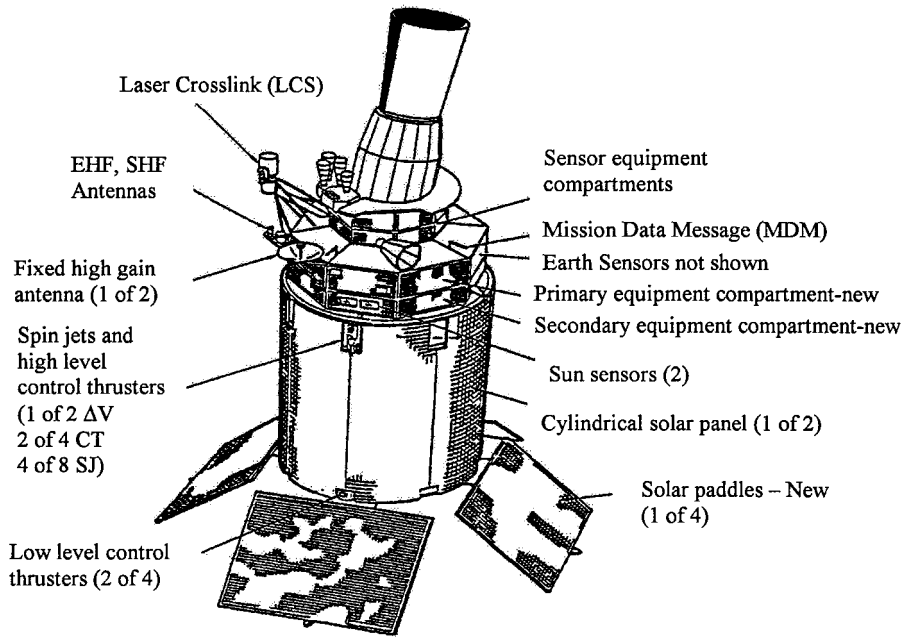

Fig. 1 DSP satellite.

Table 1 Example observational data

Index, k	Time T, s	S/C ID	Intensity I	Azimuth β, rad	Elevation η, rad	gha, rad	Declination δ, rad	Radius R, km
1	129.36	1	14.0	4.061854	0.115847	0.174532	0	42,164.17
2	130.30	2	23.0	2.427020	0.094741	1.221730	0	42,164.17
3	135.44	3	32.0	2.062181	0.142310	1.832595	0	42,164.17

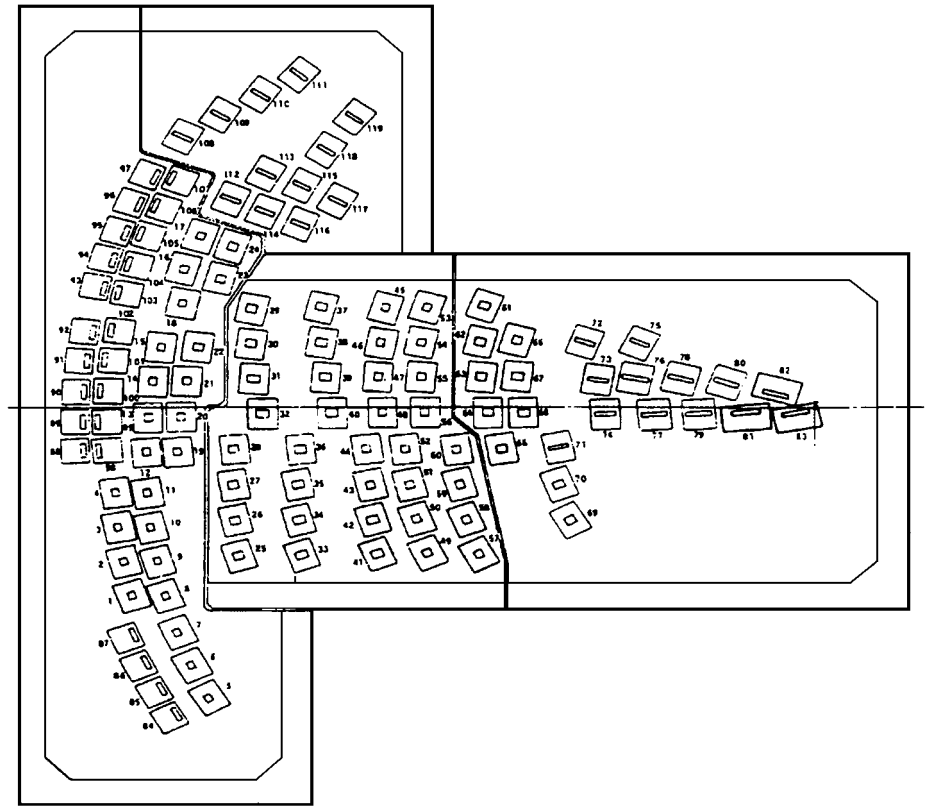

Fig. 2 PEC array.

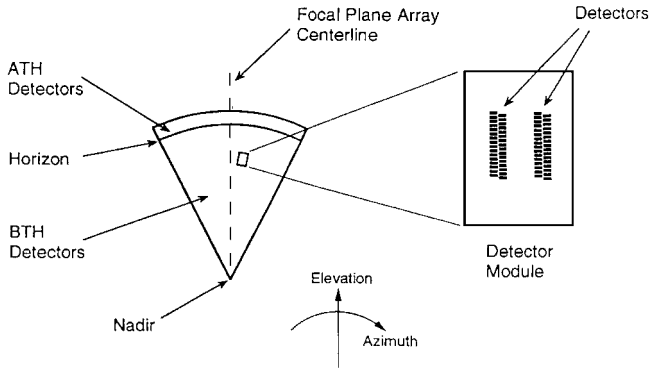

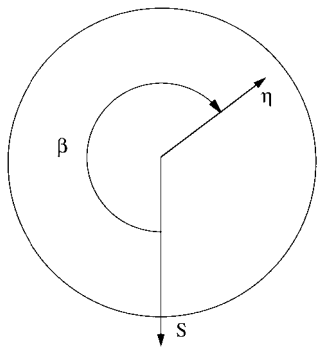

Fig. 4 Focal-plane coordinates.

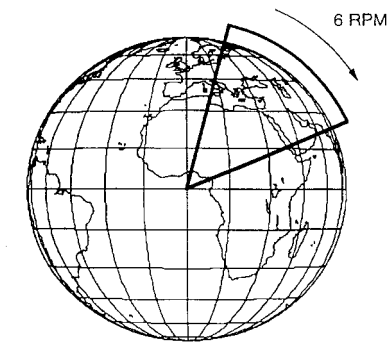

Fig. 3 Focal-plane array scanning FOV.

nominal (maximum range) vertical and horizontal ranges from the launch point as a function of time. The detected radiant intensity is compared to TBM profiles in a database, and the best match is selected as the type of TBM being observed. This selection process is complex and will be assumed to have been done correctly in this study. The downrange and altitude profiles are represented by fourth-order polynomials in time of the form

$$d_p = a_0 + a_1 t + a_2 t^2 + a_3 t^3 + a_4 t^4, \text{ downrange}$$
$$h_p = b_0 + b_1 t + b_2 t^2 + b_3 t^3 + b_4 t^4, \text{ altitude} \tag{1}$$

These coefficients are not determined by the algorithm but are assumed to be known from the typing process, i.e., perfect a priori

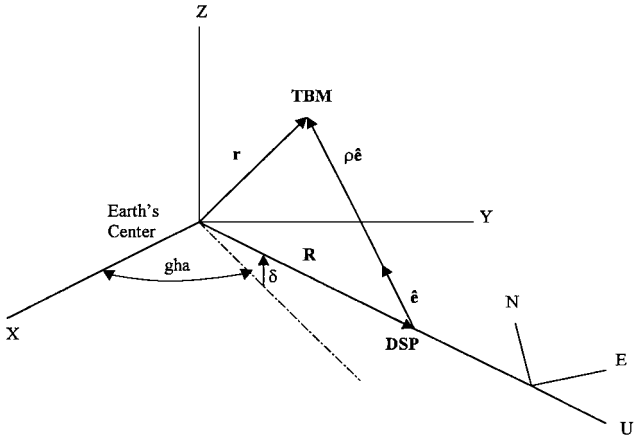

Fig. 5 Coordinate frames.

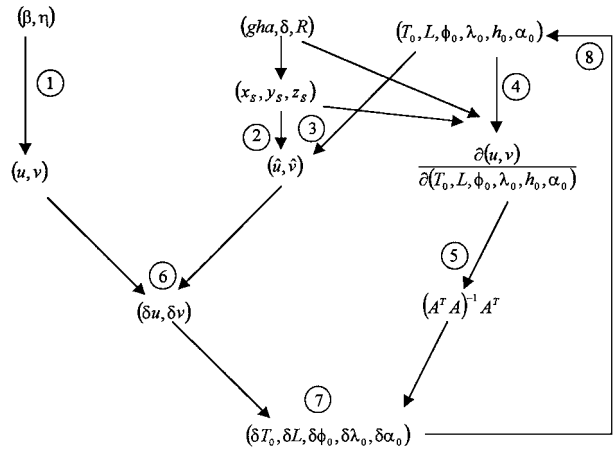

Fig. 6 Flowchart diagram of iteration process.

knowledge of the particular observed TBM's nominal trajectory. Because real-life TBMs do not fly the trajectory exactly, using the profile introduces an error. This error is ignored in this analysis because the purpose here is to determine the effects of other error sources.

A loft parameter L is used to account for trajectories above or below the nominal profile. The actual range and altitude are modeled by

$$d = (1 - 1.5L)d_p, \qquad h = (1 + L)h_p \tag{2}$$

The loft varies over ± 0.25; $L > 0$ represents a lofted trajectory, and $L < 0$ represents a depressed trajectory.

Nonlinear Least-Squares Estimation

For the estimation process, it is convenient to express the polar focal-plane observations (β, η) in focal-plane Cartesian coordinates (u, v) so that the coordinates have similar behavior with respect to errors and noise. The transformation is

$$u = -\tan\eta \sin\beta, \qquad v = -\tan\eta \cos\beta \tag{3}$$

For the nonlinear least-squares estimation, let $\boldsymbol{y}$ be the vector of observations, and let $\boldsymbol{x}$ be the tactical parameter vector, that is,

$$\begin{gathered} \boldsymbol{y}^T = (y_1, y_2, \ldots, y_n), \qquad y_k^T = (u_k, v_k) \\ \boldsymbol{x}^T = (T_0, L, \phi_0, \lambda_0, h_0, \alpha_0) \end{gathered} \tag{4}$$

The actual and calculated observations y_O and y_C are based on specific values of the tactical parameters. The nonlinear least-squares method proceeds as follows: Assume some initial values of the tactical parameters $\boldsymbol{x}_C$ (how to obtain these is discussed later), expand the equations for the observations in a Taylor series about these initial values, and retain the first term of the series:

$$\begin{gathered} \boldsymbol{y}_O(\boldsymbol{x}, t) = \boldsymbol{y}(\boldsymbol{x}_C, t) + \left.\frac{\partial \boldsymbol{y}}{\partial \boldsymbol{x}}\right|_{x=x_C} (\boldsymbol{x} - \boldsymbol{x}_C) \\ \boldsymbol{y}_O(\boldsymbol{x}, t) = \boldsymbol{y}_C + \boldsymbol{A}\delta\boldsymbol{x}, \qquad \boldsymbol{A} = \left.\frac{\partial \boldsymbol{y}}{\partial \boldsymbol{x}}\right|_{x=x_C} \end{gathered} \tag{5}$$

To find the values of the tactical parameters $\boldsymbol{x}$ that minimize the difference between the calculated observations $\boldsymbol{y}_C$ and the actual observations $\boldsymbol{y}_O$, minimize

$$\begin{gathered} Q = (\boldsymbol{y}_O - \boldsymbol{y}_C)^T \boldsymbol{W} (\boldsymbol{y}_O - \boldsymbol{y}_C) \\ Q = (\delta\boldsymbol{y} - \boldsymbol{A}\delta\boldsymbol{x})^T \boldsymbol{W} (\delta\boldsymbol{y} - \boldsymbol{A}\delta\boldsymbol{x}), \qquad \delta\boldsymbol{y} = (\boldsymbol{y}_O - \boldsymbol{y}_C) \end{gathered} \tag{6}$$

The weighting matrix $\boldsymbol{W}$ usually is taken as a diagonal matrix, where the diagonal terms are the inverse of the variances of the observations. In this analysis we have assumed that $\boldsymbol{W}$ is the identity matrix.

To find the change in the value of the tactical parameters $\delta\boldsymbol{x}$ that minimizes Q,

$$\frac{\partial Q}{\partial \delta \boldsymbol{x}} = 2\boldsymbol{A}^T \boldsymbol{W} (\delta\boldsymbol{y} - \boldsymbol{A}\delta\boldsymbol{x}) = 0 \tag{7}$$

If there are n observations, then this is a set of $2n$ equations with six unknowns. The solution is

$$\delta\boldsymbol{x} = (\boldsymbol{A}^T \boldsymbol{W} \boldsymbol{A})^{-1} \boldsymbol{A}^T \boldsymbol{W} \delta\boldsymbol{y} \tag{8}$$

The process is shown in Fig. 6. With an initial estimate of $\boldsymbol{x}$, calculate $\boldsymbol{y}_C$ and $\boldsymbol{A}$; then, with $\delta\boldsymbol{y} = \boldsymbol{y}_O - \boldsymbol{y}_C$, calculate $\delta\boldsymbol{x}$. (The initial estimate $\boldsymbol{x}$ and A are addressed in the following two sections.) With $(\boldsymbol{x}_C)_j = (\boldsymbol{x}_C)_{j-1} + \delta\boldsymbol{x}$, continue the process until the changes in $\delta\boldsymbol{x}$ become smaller than some tolerance. The resulting solution is the best estimate in the least-squares sense.

If $\boldsymbol{W}$ is the inverse of the covariance of the measurement errors, then it can be shown that the matrix

$$\boldsymbol{C} = (\boldsymbol{A}^T \boldsymbol{W} \boldsymbol{A})^{-1} \tag{9}$$

is the covariance matrix of the tactical parameters.

Initial Estimate

The initial guess of the launch point is obtained by projecting the LOS for the first observation for each of the satellites detecting the launch onto the surface of the Earth, which yields a latitude and longitude. These values then are averaged to obtain the initial guess. For example, if the first three observations are from different satellites and ϕ_i and λ_i, $i = 1, 2, 3$, are the latitudes and longitudes of the projections of the observations onto the surface of the Earth, then the initial estimates are

$$\phi_0^{(0)} = \frac{\phi_1 + \phi_2 + \phi_3}{3}, \qquad \lambda_0^{(0)} = \frac{\lambda_1 + \lambda_2 + \lambda_3}{3} \tag{10}$$

The initial estimates for L and h_0 are $L = 0$, $h_0 = 0$. As a result of the scanning sensor, cloud cover, and other factors, the TBM is not detected at launch. Based on results from known launches, the time of launch is taken as 20 s before the first observation, i.e.,

$$T_0 = T_1 - 20 \tag{11}$$

To obtain the heading, the last observations from each of the satellites are averaged in the same manner as the first to obtain

$$\phi_{\text{last}} = \frac{\phi_{n-2} + \phi_{n-1} + \phi_n}{3}, \qquad \lambda_{\text{last}} = \frac{\lambda_{n-2} + \lambda_{n-1} + \lambda_n}{3} \tag{12}$$

The heading is obtained from the great circle arc between these two points:

$$\alpha_0^{(0)} = \frac{\pi}{2} - \tan^{-1}\left[\frac{\left(\lambda_{\text{last}} - \lambda_0^{(0)}\right)\cos\phi_0^{(0)}}{\left(\phi_{\text{last}} - \phi_0^{(0)}\right)}\right] \tag{13}$$

Matrix of Partials

The matrix of partials $\boldsymbol{A}$ is best developed by decomposing it into a set of matrix multiplications. Referring to Fig. 5, the (X, Y, Z) coordinate is fixed to the Earth and has its origin at the Earth's center, and the (U, E, N) coordinate system has its origin at the DSP satellite. Defining

$$\boldsymbol{s} = (\phi, \lambda, h)^T, \qquad \boldsymbol{r} = (x, y, z)^T, \qquad \boldsymbol{w} = (U, E, N)^T \tag{14}$$

$$\boldsymbol{A}_1 = \frac{\partial \boldsymbol{s}}{\partial \boldsymbol{x}}, \qquad \boldsymbol{A}_2 = \frac{\partial \boldsymbol{r}}{\partial \boldsymbol{s}}, \qquad \boldsymbol{A}_3 = \frac{\partial \boldsymbol{w}}{\partial \boldsymbol{r}}, \qquad \boldsymbol{A}_4 = \frac{\partial \boldsymbol{y}}{\partial \boldsymbol{w}} \tag{15}$$

$$\boldsymbol{A} = \boldsymbol{A}_4 \boldsymbol{A}_3 \boldsymbol{A}_2 \boldsymbol{A}_1 \tag{16}$$

Equation (16) decomposes $\boldsymbol{A}$ into four matrices, which are relatively easy to derive analytically. They are given in the Appendix. The reader is referred to Ref. 2 for their derivation.

Burnout Time Estimation

The estimation T_{bo} is based on $t_{\max}$, T_{last}, and T_{next}, had it occurred. The maximum burn time according to the profile is

$$T_{\max} = T_0 + t_{\max} \tag{17}$$

Two cases can occur:

1) If $T_{\max} > T_{\text{next}}$, then

$$T_{\text{bo}} = T_{\text{last}} + \frac{T_{\text{next}} - T_{\text{last}}}{2} \tag{18}$$

2) If $T_{\max} < T_{\text{next}}$, then

$$T_{\text{bo}} = T_{\text{last}} + \frac{T_{\max} - T_{\text{last}}}{2} \tag{19}$$

State Vector Generation

The state vector completely defines the TBM's position and velocity. With the tactical parameters and burnout time estimates, the altitude and range at burnout are obtained using Eqs. (1) and (2) with

$$t_{\text{bo}} = T_{\text{bo}} - T_0 \tag{20}$$

Using

$$\theta_{\text{bo}} = d_{\text{bo}} / R_e \tag{21}$$

the position at burnout is

$$\phi_{\text{bo}} = (\pi/2) - \cos^{-1}(\cos\theta_{\text{bo}} \sin\phi_0 + \sin\theta_{\text{bo}} \cos\phi_0 \cos\alpha_0)$$
$$\lambda_{\text{bo}} = \lambda_0 + \sin^{-1}\left(\frac{\sin\theta_{\text{bo}} \sin\alpha_0}{\cos\phi_{\text{bo}}}\right), \qquad \text{alt}_{\text{bo}} = h_0 + h_{\text{bo}} \tag{22}$$

The velocity at burnout is

$$V_{\text{bo}} = \sqrt{\dot{d}^2 + \dot{h}^2}, \qquad \gamma_{\text{bo}} = \tan^{-1}(\dot{h}/\dot{d})$$
$$\alpha_{\text{bo}} = \sin^{-1}\left(\frac{\cos\phi_0 \sin\alpha_0}{\cos\phi_{\text{bo}}}\right), \qquad \dot{d} = \frac{\partial d}{\partial t}, \qquad \dot{h} = \frac{\partial h}{\partial t} \tag{23}$$

The state vector at burnout is $(\phi_{\text{bo}}, \lambda_{\text{bo}}, h_{\text{bo}}, V_{\text{bo}}, \gamma_{\text{bo}}, \alpha_{\text{bo}})^T$.

Impact Position and Time

The ballistic trajectory is modeled in three phases[5]: powered flight, which is the portion the DSP observes; free flight, which is a portion of an elliptic orbit or ballistic trajectory; and re-entry, which is the portion in which atmospheric drag becomes significant until missile impact. The powered flight is modeled with the TBM profile polynomials presented earlier [Eq. (1)]. The ellipse traced during free flight is simulated using inertial two-body mechanics. Atmospheric drag effects during the re-entry phase are not specifically calculated in this model but are accounted for somewhat by assuming that the distance traveled over the Earth from re-entry to impact is the same as from launch to burnout. This is the same as assuming that the Earth-central angles are the same, i.e., $\theta_{\text{re}} = \theta_{\text{bo}}$. These are approximations, but their effect should be small for the error analysis. That is, neglecting the effect of the atmosphere should have a very small effect on the error due to error sources addressed here. The effect of the atmosphere is not negligible if one is concerned with the actual trajectory.[2]

Error Sources

Each error source usually has one or more underlying causes. For example, the LOS error is a result of attitude errors and focal-plane misalignments. A complete error analysis would break each error source down to its fundamental level and model each level correctly. In this section, some of the underlying causes of the overall sources are identified, but in these analyses, only the overall error magnitudes are analyzed. The errors are grouped into three types: time, LOS, and satellite position. Time errors can be caused simply by having more than one clock referenced as a source of time measurement. Imperfect synchronization between clocks' time and time passage rate are obvious error sources. Time delays caused by radio transmission of data due to distance, atmospheric refraction, and relative-motion Doppler effects may add another time error. The magnitude of time errors is relatively small and getting smaller as time measurements are being made continually.

LOS measurement errors can arise from many sources, primarily attitude uncertainties and IR radiation measurement errors. Any attitude control system inaccuracy effects are amplified by the geosynchronous altitude. The knowledge of the telescope alignment with the satellite's reference frame is defined by the design and manufacturing of the DSP satellite and changes slightly with thermal variations. The IR radiation measurements of intensity and angle of arrival also have several underlying error sources. Locations of the individual PECs on the focal-plane array are recorded in what is termed the focal-plane vector table (FPVT). The positions of the PECs change as the satellite heats and cools with varying sun–satellite orientations, causing a warping of the focal plane, but the FPVT does not account for the changes in real time. In addition, detector noise, refraction, and IR attenuation due to clouds and water vapor all add to the total measurement error.

Satellite position measurements from the AFSCN are used to update the ephemeris once per week. The ephemeris is propagated from the time of update to estimate the satellite position for the next week. The measurements are, of course, inexact, and the resulting ephemeris error grows with time during the one-week prediction interval.

Because the missile profile, Eqs. (1) and (2), is an approximation of an average trajectory for each missile class, it is a source of error. The profiles can be a major error source. However, this analysis does not consider this error source and assumes the profile to be perfect.

Another source of error is the burnout time. This error is not the result of an error in the system but is the result of the 10-s scan period. The error in the burnout time is considered in this analysis.

Keeping all of these underlying components in mind, the errors are modeled in the tactical parameter algorithm. The real-world error-component magnitudes, bias, and random distributions may be different from those simulated, but the overall effects manifest themselves in a manner close to the error models. It should be possible to extrapolate the results obtained in this study to different errors by properly scaling the different magnitudes and distributions. It must be emphasized that the goal of this study is not to exactly determine the tactical parameters at launch, state vector at burnout, or impact time and position. The purpose is to determine the contribution of the various error sources to these values, and this can be done with approximate models for the errors. If the intended goal is to calibrate the system to eliminate bias errors, then the error sources must be modeled more exactly to determine what is observable.

Results

The algorithm previously described was programmed into MATLAB™. Three error sources—time, satellite position, and LOS—were simulated and added to the observational data, first

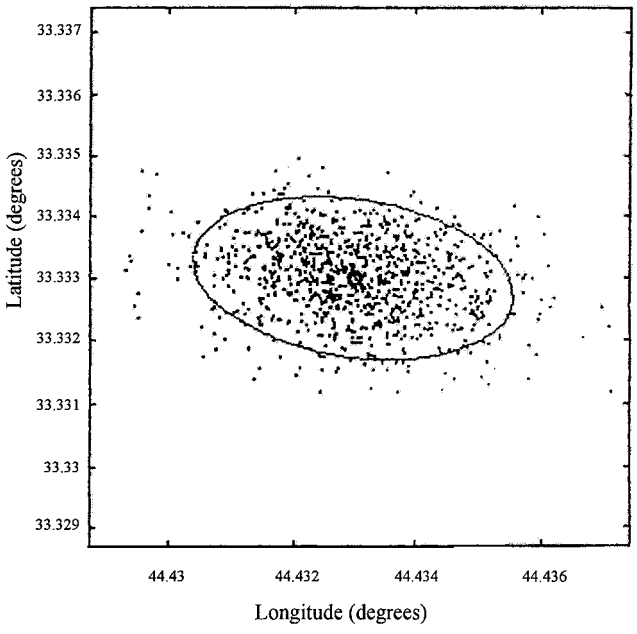

Fig. 7 Launch-position error ellipse.

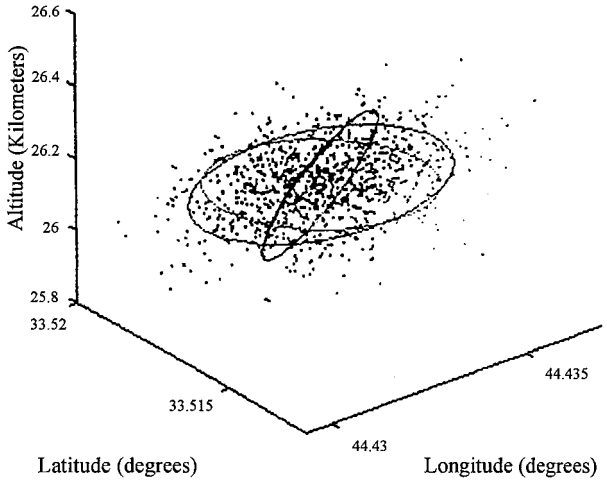

Fig. 8 Burnout-position error ellipsoid.

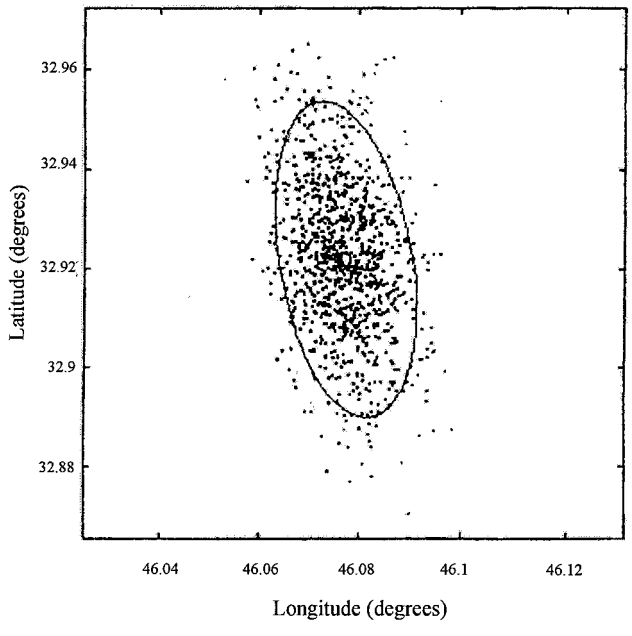

Fig. 9 Impact-position error ellipse.

separately and then combined. The effects of the errors on the results are analyzed at three points: launch position, burnout position, and impact position. Five Middle Eastern capital cities—Aden, Baghdad, Damascus, Riyadh, and Tehran—were chosen as fictitious launch sites to determine the effects of TBM launch position on the accuracy of the results. Results are presented for only three of the cities—Baghdad, Aden, and Damascus—but the results are representative of all five cities. Reference 2 presents the results for all five cities. Except when noted, this analysis assumed three DSP satellites in geostationary orbit at longitudes 10°E, 70°E, and 105°E. The approach was Monte Carlo with 1000 runs for each condition.

The model for the time error is a random uniform distribution between 0 and 1 ms. For satellite position, a random normal distribution with zero mean and standard deviation of 200 m was added to each component, radial, in track, and cross track. A random distribution of 200 m in each of the components is equivalent to a one-standard-deviation sphere of 346 m. The LOS error was modeled as a random normal distribution with a standard deviation of 5 μrad, added to both the β and η components. The values used for the error sources are representative of what can occur.

Figures 7–9 show for a due-east launch from Baghdad the distribution and error ellipse for the launch point, burnout point, and impact point, respectively. The estimated impact point (no error impact point) is the one resulting from the model used in this paper, not the impact point that would occur if atmospheric effects and the other neglected factors were included. The error ellipse (ellipsoid) is the figure defined by[6]

$$z^T C^{-1} z = 1 \tag{24}$$

where z is the vector representing the variables in question, e.g., latitude, longitude, and altitude. Recall that the time error and the burnout time are not Gaussian, and so the covariance matrix does not represent a Gaussian error distribution. Figure 8 is an ellipsoid because the burnout point is three dimensional. The three orthogonal ellipses for each set of two axes are shown.

The data for the 300-km TBM were collated by city, heading, and error source. The area (volume) of the error ellipse (ellipsoid) for each of the three points for each of the three error sources as a function of the heading are shown in Figs. 10–18. Figures 19–21 show the combined error effects for the three points. Each figure has two curves for the two launch points (cities). Immediately apparent is that the launch point has very little effect on the size of the error ellipses and ellipsoids. Also evident is that the observational geometry and TBM heading have a large effect on the ellipsoid size.

Table 2 summarizes the results by showing the minimum, mean, and maximum area (volume) over all headings for each error source for the three points. It is evident from the results that the error sources can be ranked in order of effect: 1) LOS errors, 2) satellite position errors, and 3) time errors.

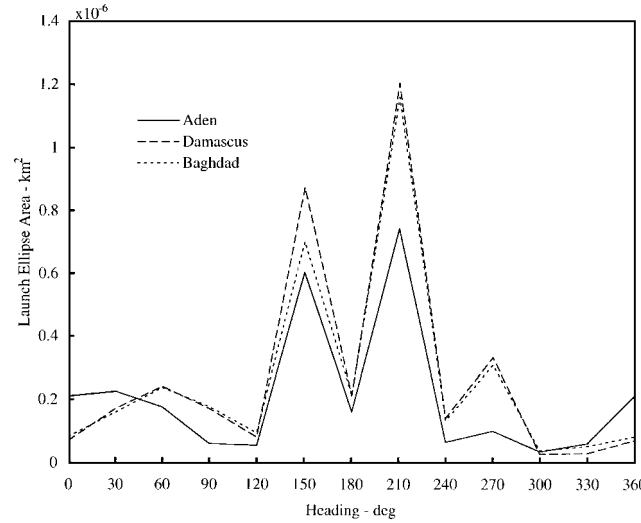

Fig. 10 Time-error effects on launch ellipse area.

Table 2 Error ellipse areas and volumes

	Launch ellipse area, km^2			Burnout ellipsoid volume, km^2			Impact ellipse area, km^2		
Error	Min	Mean	Max	Min	Mean	Max	Min	Mean	Max
Time	3.26e-8	2.59e-7	1.22e-6	2.9e-11	3.6e-10	1.33e-9	1.57e-6	2.61e-5	1.41e-4
Satellite position	3.77e-3	5.27e-3	8.68e-3	6.04e-4	1.14e-3	2.32e-3	6.12e-3	7.92e-3	3.27e-1
LOS	2.97e-2	8.45e-2	1.83e-1	2.37e-2	9.33e-2	2.09e-1	3.05e-0	1.02e-1	1.95e-1
Combined	3.91e-1	1.01e-1	2.97e-1	4.44e-2	1.25e-1	4.50e-1	3.35e-0	1.38e-1	4.06e-1

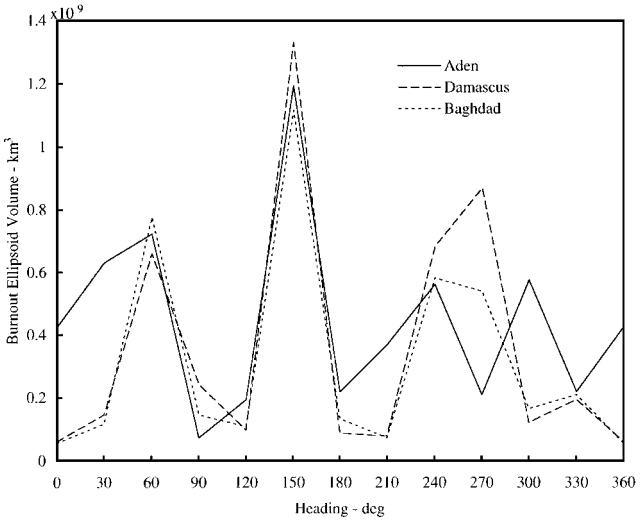

Fig. 11 Time-error effects on burnout ellipsoid volume.

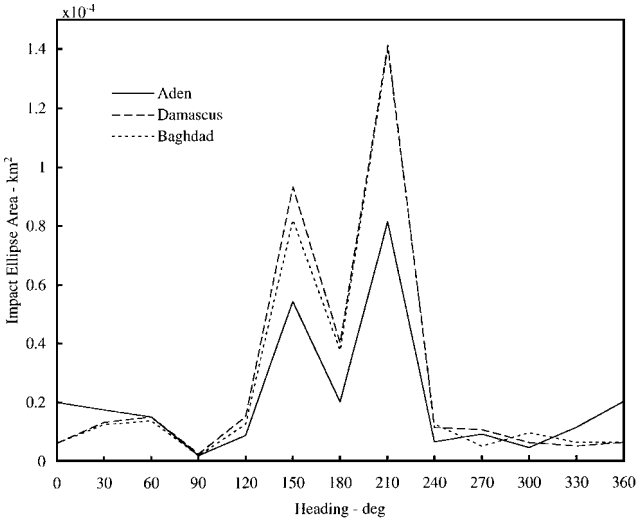

Fig. 12 Time-error effects on impact ellipse area.

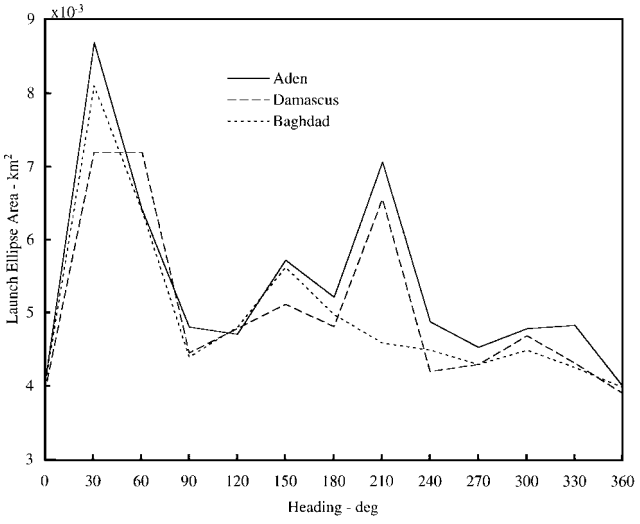

Fig. 13 Satellite-position error effects on launch ellipse area.

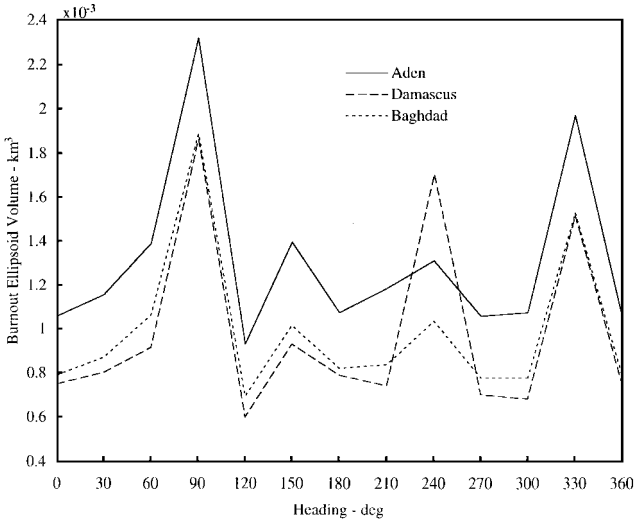

Fig. 14 Satellite-position error effects on burnout ellipsoid volume.

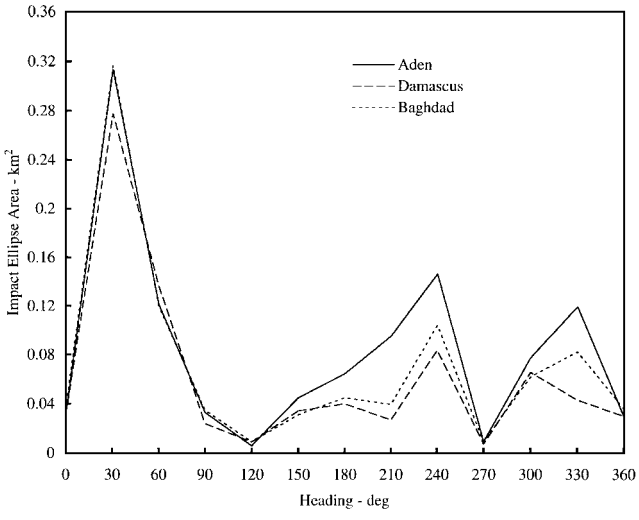

Fig. 15 Satellite-position error effects on impact ellipse area.

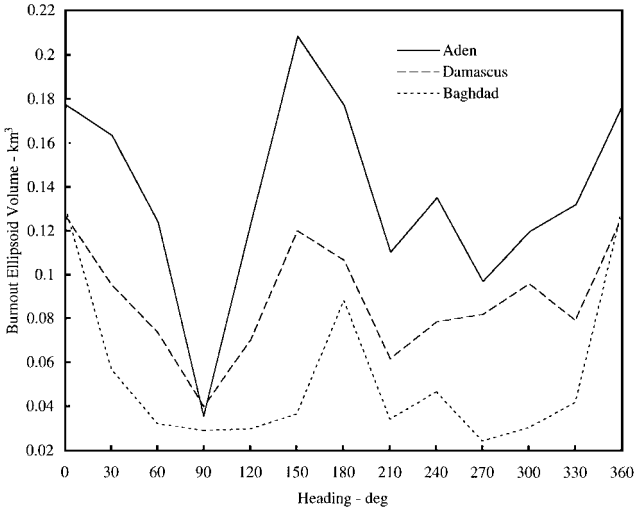

Fig. 16 LOS-error effects on launch ellipse area.

Table 3 Various-case comparison

	Launch ellipse area, km^2			Burnout ellipsoid volume, km^2			Impact ellipse area, km^2		
Error	Min	Mean	Max	Min	Mean	Max	Min	Mean	Max
Bagcom	4.21e-2	1.01e-1	2.74e-1	4.46e-2	1.09e-1	2.60e-1	3.83e-0	1.40e-1	4.04e-1
Synchr.	4.40e-2	7.07e-2	1.10e-1	2.09e-2	4.89e-2	8.61e-2	3.94e-0	7.82e-0	1.52e-0
Molniya	4.39e-2	7.58e-2	1.25e-1	2.61e-2	5.57e-2	1.04e-1	2.91e-0	7.96e-0	1.85e-1
10-s scan	4.21e-2	1.01e-1	2.74e-1	4.46e-2	1.09e-1	2.60e-1	3.83e-0	1.40e-1	4.04e-1
7.5-s scan	2.62e-2	7.44e-2	1.95e-1	2.53e-2	4.55e-2	1.09e-1	4.03e-0	8.72e-0	2.08e-1
5.0-s scan	2.48e-2	5.02e-2	1.52e-1	1.23e-2	2.52e-2	6.52e-2	2.52e-0	5.84e-0	1.64e-1
2.5-s scan	1.18e-2	2.36e-2	3.48e-2	5.05e-3	9.21e-3	1.31e-2	1.03e-0	2.95e-0	4.58e-0

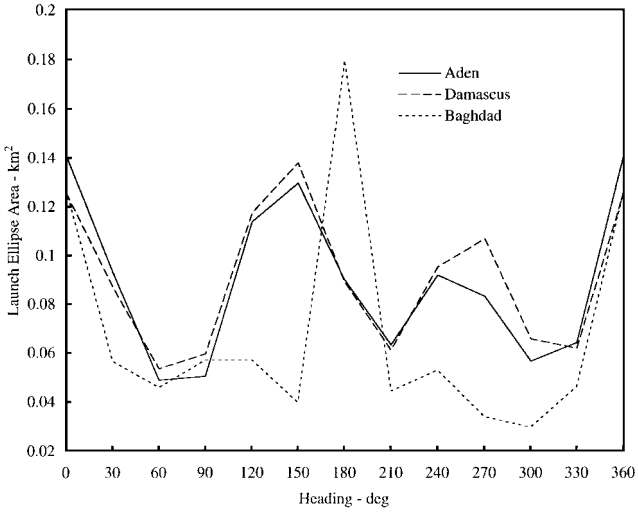

Fig. 17 LOS-error effects on burnout ellipsoid volume.

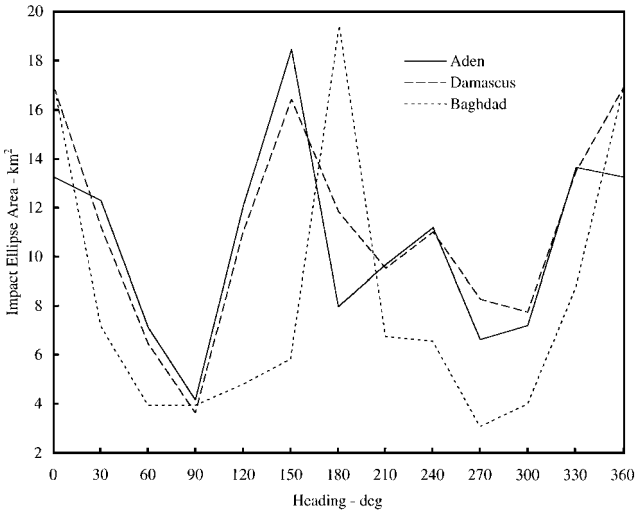

Fig. 18 LOS-error effects on impact ellipse area.

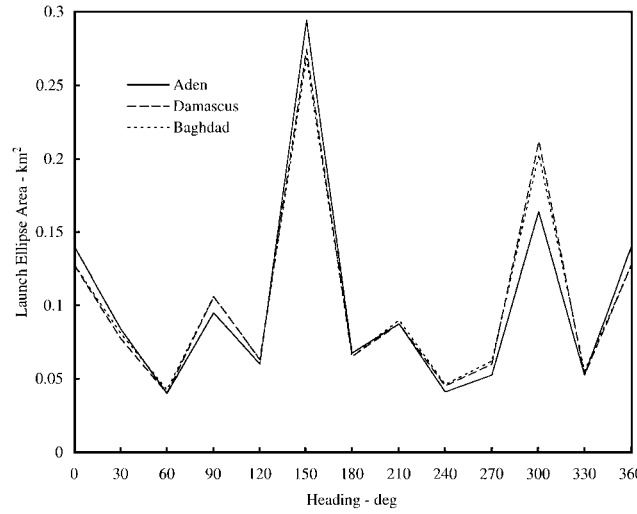

Fig. 19 Combined error effects on launch error ellipse.

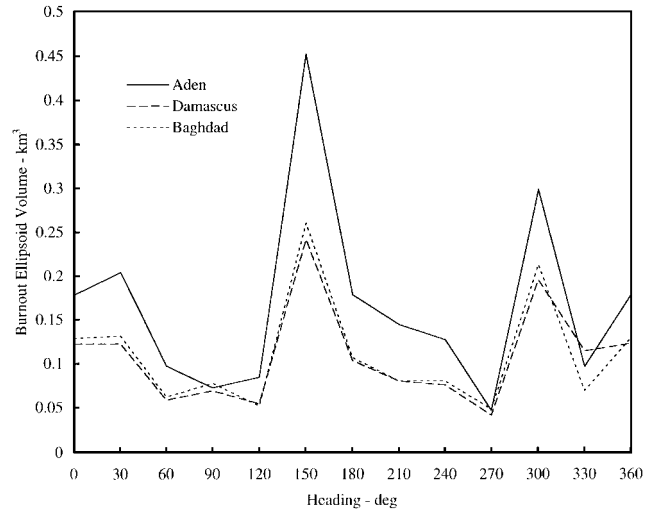

Fig. 20 Combined error effects on burnout error ellipsoid.

Taking advantage of the ease of modifying the MATLAB code, various changes to the present DSP system model were made to determine the effects on the accuracy of the results. For these cases the launch site was Baghdad and the observational data were modified by the combined error sources.

The first case is the control case with nominal parameters and is denoted by Bagcom to represent Baghdad combined errors, and it is used as a baseline case for comparison. The second case, Synchr., shows the effect of synchronizing the spins of the satellites so that the satellites scan the area of interest within 1 s of each other. In the third case, Molniya, a third satellite at 70°E GHA and 63.4° latitude replaced the DSP satellite at the same longitude to simulate a Molniya + geostationary viewing geometry. The purpose here was to evaluate the effect of better triangulation of the launch. The remaining cases simulated faster scan periods from 10 s down to 2.5 s. The results are shown in Table 3.

The first two modifications have the effect of decreasing the mean areas and volume by about 30–50%. A decrease is expected for the Molniya case because two satellites on the equator and one at high latitude provide better viewing geometry. The synchronized spin results were somewhat of a surprise, however. The effect on the launch ellipse area is expected, but because the burnout time estimate should be less accurate, it would be expected that the burnout ellipsoid volume and impact ellipsoid area would increase. However, they decreased. More research is needed in this area.

Increasing the scan rate has two positive effects: More data are obtained during the boost phase, allowing for a better trajectory estimate, and a better estimate of the burnout time is obtained. The decreases in the launch ellipse area and the impact ellipse area are essentially linear with decreasing scan rate, and the burnout ellipsoid volume decrease is quadratic.

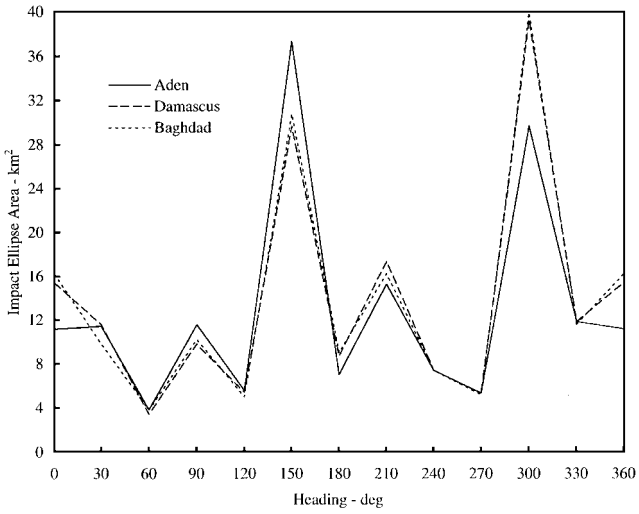

Fig. 21 Combined error effects on impact error ellipse.

Conclusions

An analysis of the errors in the estimated launch point, burnout point, and impact point of a TBM because of system error sources has been performed for a system of launch detection satellites in geosynchronous orbit. The TALON SHIELD/ALERT state vector estimation algorithm was used to estimate the launch point, burnout point, and impact point. System errors were modeled and introduced into the algorithm to determine the effects on accuracy of the final results. The errors were broadly categorized as errors in time, satellite position, and LOS. The relative magnitudes of the error effects, listed largest to least, are as follows:

LOS—using a zero mean, 5-μrad standard deviation normal error distribution in focal plane coordinates,

Satellite position—using a zero-mean, 200-m standard-deviation normal error distribution in satellite position coordinates,

Time—using a uniform error distribution between zero and one ms.

As expected, the effects behave independently, and the principle of superposition can be used.

Appendix: Partial Derivatives

In this Appendix the partial derivatives are presented. From Eqs. (4) and (14–16),

$$\boldsymbol{y} = (u_1, v_1, u_2, v_2, \ldots, u_n, v_n)^T$$

$$\boldsymbol{x} = (T_0, L_0, \phi_0, \lambda_0, h_0, \alpha_0)^T \tag{A1}$$

$$\boldsymbol{s} = (\phi, \lambda, h)^T, \qquad \boldsymbol{r} = (x, y, z)^T, \qquad \boldsymbol{w} = (U, E, N)^T$$

$$\boldsymbol{A}_1 = \frac{\partial \boldsymbol{s}}{\partial \boldsymbol{x}}, \qquad \boldsymbol{A}_2 = \frac{\partial \boldsymbol{r}}{\partial \boldsymbol{s}}, \qquad \boldsymbol{A}_3 = \frac{\partial \boldsymbol{w}}{\partial \boldsymbol{r}}, \qquad \boldsymbol{A}_4 = \frac{\partial \boldsymbol{y}}{\partial \boldsymbol{w}} \tag{A2}$$

$$\boldsymbol{A} = \boldsymbol{A}_4 \boldsymbol{A}_3 \boldsymbol{A}_2 \boldsymbol{A}_1 \tag{A3}$$

$$\boldsymbol{A}_1 = \begin{bmatrix} \dfrac{\partial d}{\partial T_0}\dfrac{\cos\alpha_0}{r_{\text{eff}}} & -\dfrac{1.5 d_p \cos\alpha_0}{r_{\text{eff}}} & 1 & 0 & 0 & -\dfrac{d\sin\alpha_0}{r_{\text{eff}}} \\ \dfrac{\partial d}{\partial T_0}\dfrac{\sin\alpha_0}{r_{\text{eff}}\cos\phi_0} & -\dfrac{1.5 d_p \sin\alpha_0}{r_{\text{eff}}\cos\phi_0} & 0 & 1 & 0 & \dfrac{d\cos\alpha_0}{r_{\text{eff}}\cos\phi_0} \\ \dfrac{\partial h}{\partial T_0} & h_p & 0 & 0 & 1 & 0 \end{bmatrix} \tag{A4}$$

$\boldsymbol{A}_2$ can be approximated by

$$\boldsymbol{A}_2 = \begin{bmatrix} -(r_{\text{eff}}+h)\sin\phi\cos\lambda & -(r_{\text{eff}}+h)\cos\phi\sin\lambda & \cos\phi\cos\lambda \\ -(r_{\text{eff}}+h)\sin\phi\sin\lambda & +(r_{\text{eff}}+h)\cos\phi\cos\lambda & \cos\phi\sin\lambda \\ (r_{\text{eff}}+h)\cos\phi & 0 & \sin\phi \end{bmatrix} \tag{A5}$$

$\boldsymbol{A}_3$ is the transformation between (XYZ) and (UEN):

$$\boldsymbol{A}_3 = \begin{bmatrix} \cos\delta_k & 0 & \sin\delta_k \\ 0 & 1 & 0 \\ -\sin\delta_k & 0 & \cos\delta_k \end{bmatrix} \begin{bmatrix} \cos(\text{gha}_k) & \sin(\text{gha}_k) & 0 \\ -\sin(\text{gha}_k) & \cos(\text{gha}_k) & 0 \\ 0 & 0 & 1 \end{bmatrix} \tag{A6}$$

From

$$u_k = -E_k/U_k, \qquad v_k = -N_k/U_k \tag{A7}$$

$$\boldsymbol{A}_4 = \begin{bmatrix} E_k/U_k^2 & -1/U_k & 0 \\ N_k/U_k^2 & 0 & -1/U_k \end{bmatrix} \tag{A8}$$

References

[1] Rodrigues, L. J., "Defense Support Program Station Upgrades Not Based on Validated Requirements," *GAO Report to the Acting Secretary of the Air Force*, U.S. General Accounting Office, Washington, DC, 1993.

[2] Beaulieu, M. R., "Launch Detection Satellite System Engineering Error Analysis," M.S. Thesis, Dept. of Aeronautics and Astronautics, U.S. Naval Postgraduate School, Monterey, CA, 1996.

[3] Danis, N. J., "Space-Based Tactical Ballistic Missile Launch Parameter Estimation," *IEEE Transactions on Aerospace and Electronic Systems*, Vol. 29, No. 2, 1993, pp. 412–424.

[4] Bontrager, M. D., "Defense Support Program," *Space Operations Orientation Course Handbook*, U.S. Air Force Space Command, Colorado Springs, CO, 1993, pp. 179–190.

[5] Bates, R. R., Mueller, D. D., and White, J. E., *Fundamentals of Astrodynamics*, Dover, New York, 1971, pp. 279–296.

[6] Torrieri, D. J., "Statistical Theory of Passive Location Systems," *IEEE Transactions on Aerospace and Electronic Systems*, Vol. 20, No. 2, 1994, pp. 183–198.

J. D. Gamble
Associate Editor